

Spin correlations and exchange in square lattice frustrated ferromagnets

M. Skoulatos,^{1,*} J.P. Goff,² C. Geibel,³ E.E. Kaul,³ R. Nath,³ N. Shannon,⁴
B. Schmidt,³ A.P. Murani,⁵ P.P. Deen,⁵ M. Enderle,⁵ and A.R. Wildes⁵

¹*Helmholtz Centre Berlin for Materials and Energy, Glienicker Str. 100, 14109 Berlin, Germany*

²*Department of Physics, Royal Holloway, University of London, Egham, Surrey TW20 0EX, United Kingdom*

³*Max-Planck Institute for Chemical Physics of Solids, Nöthnitzer Str. 40, Dresden 01187, Germany*

⁴*H.H. Wills Physics Laboratory, University of Bristol, Bristol BS8 1TL, United Kingdom*

⁵*Institut Laue-Langevin, 156X, 38042 Grenoble Cedex, France*

(Dated: November 30, 2018)

The J_1 - J_2 model on a square lattice exhibits a rich variety of different forms of magnetic order that depend sensitively on the ratio of exchange constants J_2/J_1 . We use bulk magnetometry and polarized neutron scattering to determine J_1 and J_2 unambiguously for two materials in a new family of vanadium phosphates, $\text{Pb}_2\text{VO}(\text{PO}_4)_2$ and $\text{SrZnVO}(\text{PO}_4)_2$, and we find that they have ferromagnetic J_1 . The ordered moment in the collinear antiferromagnetic ground state is reduced, and the diffuse magnetic scattering is enhanced, as the predicted bond-nematic region of the phase diagram is approached.

PACS numbers: 75.50.y; 75.40.Cx; 75.40.Gb; 75.30.Et; 75.25.+z

Keywords: $J_1 - J_2$ model; Diffuse scattering; Collinear antiferromagnet; Ferromagnetic exchange

The square-lattice $S = 1/2$ Heisenberg antiferromagnet with nearest-neighbour (NN) exchange constant J_1 and next-nearest-neighbour (NNN) exchange J_2 , has long served as a paradigm for the two-dimensional frustrated magnetism (for a review see Ref. [1]). It is described by the following Hamiltonian:

$$\mathcal{H} = J_1 \sum_{\langle i,j \rangle_1} \mathbf{S}_i \cdot \mathbf{S}_j + J_2 \sum_{\langle i,k \rangle_2} \mathbf{S}_i \cdot \mathbf{S}_k \quad (1)$$

where $\langle i,j \rangle_1$ and $\langle i,k \rangle_2$ refer to pairs of NN and NNN respectively. The so-called $J_1 - J_2$ model first came to prominence due to its relevance to the high-temperature superconducting cuprates, and the recent discovery of high- T_c superconductivity in pnictides [2, 3] has increased interest in this model, since it may play a key role for the magnetism on the square Fe sublattice [4].

The frustrated square lattice model is characterized by the frustration ratio $\alpha = J_2/J_1$, and the energy scale is given by $J_c = \sqrt{J_1^2 + J_2^2}$. When the exchange constants are antiferromagnetic (AF) and $\alpha \approx 0.5$ the ground state is believed to be a valence bond solid (VBS) in which spins form tightly bound singlets on nearest-neighbour bonds [5]. On the other hand, recent calculations for ferromagnetic (FM) J_1 and AF J_2 predict d -wave bond-nematic order for $\alpha \approx -0.5$ [6, 7]. The calculated phase diagram is shown schematically in Fig. 1.

There are now several experimental realizations of spin-1/2 magnets on a square-lattice where both J_1 and J_2 interactions play an important role. The first examples, Li_2VOXO_4 ($X = \text{Si}, \text{Ge}$), are collinear antiferromagnets (CAF) with AF exchange $J_2 \gg J_1$ [8, 9, 10, 11, 12, 13, 14, 15], whereas VOMoO_4 [16] and PbVO_3 are Néel antiferromagnets (NAF) with AF exchange $J_2 \ll J_1$ [17, 18]. In contrast, the new family of vanadium phosphates $\text{AA}'\text{VO}(\text{PO}_4)_2$ ($A, A' = \text{Pb}, \text{Zn}, \text{Sr}$,

Ba, Cd) [19, 20, 21, 22] and $(\text{CuX})\text{LaNb}_2\text{O}_7$ ($X = \text{Cl}, \text{Br}$) [23, 24] have been argued to be frustrated ferromagnets with FM J_1 and AF J_2 .

In order to explore this phase diagram, accurate control of α is required. Until now it has proved difficult to determine the exchange constants accurately using bulk

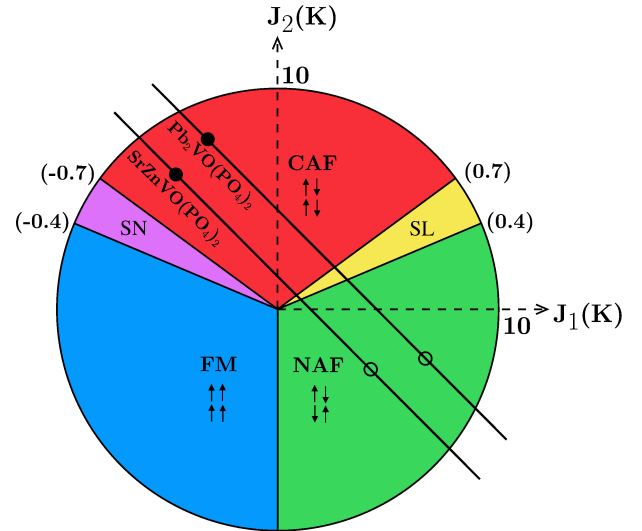


FIG. 1: Calculated phase diagram for the general $J_1 - J_2$ model, locating $\text{Pb}_2\text{VO}(\text{PO}_4)_2$ and $\text{SrZnVO}(\text{PO}_4)_2$. The values of α in parentheses are the phase boundaries determined by exact diagonalization [5, 7]. At these values, zero-point fluctuations destroy the relevant order parameter. The yellow area corresponds to the valence bond solid (VBS) regime, the purple zone to the bond-nematic (d -BN) region [6, 7, 25]. The straight lines are obtained from the Curie-Weiss temperatures, and the circles are obtained from the maxima in susceptibility, as described in the text. The filled circles are the solutions selected using polarized neutrons.

thermodynamic properties, and this is reflected by the wide variation reported for α for individual compounds in the literature. The determination of α from thermodynamic quantities alone is undermined by the fact that $J_1 + J_2$ and $|J_1 + J_2|$, but not $J_1 - J_2$ are well determined.

Here we present combined bulk magnetization and polarized neutron scattering studies of $\text{Pb}_2\text{VO}(\text{PO}_4)_2$ and $\text{SrZnVO}(\text{PO}_4)_2$. The determination of the magnetic structures in the ground state, and the comparison of the diffuse neutron scattering intensity in the paramagnetic phase with high-temperature series expansions (HTSE) provides an unambiguous determination of the exchange constants J_1 and J_2 . We are also able to explore the consequences for the spin correlations of the approach to a quantum disordered region of the phase diagram.

Large powder samples were synthesized at the Max-Planck Institute for Chemical Physics of Solids in Dresden by the solid state reaction method, in order to avoid multi-phase composition for these compounds. The quasielastic neutron experiments were performed on the D7 diffuse scattering spectrometer at the Institut Laue-Langevin (ILL) in Grenoble, with a fixed incident wavelength of $\lambda = 3.1 \text{ \AA}$ corresponding to an energy window of 8.5 meV. XYZ polarization analysis was employed to separate magnetic signal from the coherent structural and incoherent scattering [26]. Polarized inelastic neutron scattering measurements were performed using the IN20 triple-axis spectrometer of the ILL, in order to confirm the energy scale of the system. Scans of energy transfer were performed at various reciprocal lattice points, Q , and temperatures, T , and in all cases the excitations were found to be within $\pm 4 \text{ meV}$. Thus the measurements on D7 integrate over the full spectral energy range to yield the structure factor, $S(Q)$. The bulk magnetisations of $\text{Pb}_2\text{VO}(\text{PO}_4)_2$ and $\text{SrZnVO}(\text{PO}_4)_2$ were measured using a SQUID magnetometer at the University of Liverpool.

$\text{Pb}_2\text{VO}(\text{PO}_4)_2$ crystallizes in the monoclinic system

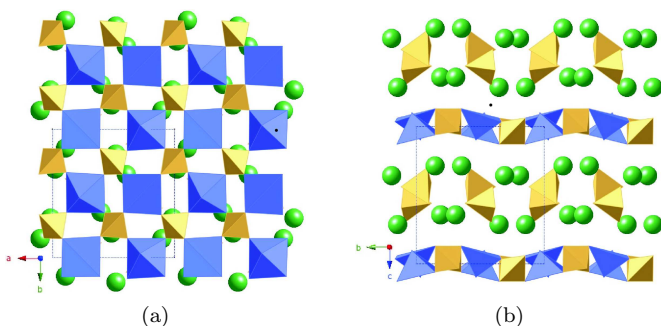


FIG. 2: The structure of $\text{Pb}_2\text{VO}(\text{PO}_4)_2$ contains corrugated layers formed by VO_5 square pyramids (blue), oriented in alternating directions in a chessboard fashion. The pyramids are connected by tetrahedral PO_4 groups (yellow). The layers are separated by the Pb atoms (green) and isolated PO_4 tetrahedra. Projections shown are for a) ab and b) bc planes.

with spacegroup $P2_1/a$ and lattice parameters $a = 8.747(4) \text{ \AA}$, $b = 9.016(5) \text{ \AA}$, $c = 9.863(9) \text{ \AA}$ and $\beta = 100.96(4)^\circ$ [20, 27]. Two projections of the $\text{Pb}_2\text{VO}(\text{PO}_4)_2$ structure are shown in Fig. 2. The structure contains corrugated layers formed by VO_5 square pyramids oriented in alternating directions in a chessboard fashion. The pyramids are connected by tetrahedral PO_4 groups. The layers are buckled along the b -axis. The square bases of the similarly oriented pyramids are located approximately at the same level. The magnetic $[\text{VOPO}_4]$ layers are well separated ($\sim 10 \text{ \AA}$) by non-magnetic Pb atoms and isolated PO_4 tetrahedra, indicating a quasi-2D character for the system. $\text{SrZnVO}(\text{PO}_4)_2$ shares many characteristics with its relative $\text{Pb}_2\text{VO}(\text{PO}_4)_2$. Their structural relationship is the replacement of the two Pb^{2+} cations by Sr^{2+} and Zn^{2+} . Again, it forms a two-dimensional square lattice of V^{4+} ions with competing interactions leading to frustration. The profound structural similarities with $\text{Pb}_2\text{VO}(\text{PO}_4)_2$ attracted our interest since small changes introduced by the cationic substitution can tune the magnetic exchanges J_1 and J_2 and thus the frustration ratio. $\text{SrZnVO}(\text{PO}_4)_2$ crystallises in the orthorhombic system with spacegroup $Pbca$ and lattice parameters $a = 9.0660 \text{ \AA}$, $b = 9.0117 \text{ \AA}$ and $c = 17.5130 \text{ \AA}$ [27, 28]. The main difference between the two compounds' space groups arises from the way the VOPO_4 layers are stacked along the c -axis.

The polycrystalline samples were measured under an applied field of 1000 Oe, giving the results of Fig. 3. For $T > 50 \text{ K}$, $\chi(T)$ is characterised by a paramagnetic Curie-Weiss (CW) behaviour. Below that, $\chi(T)$ passes through a broad maximum that is characteristic of a low-dimensional magnet, peaked at $T_{\text{Max}} \sim 8.5 \text{ K}$ and 6.3 K for $\text{Pb}_2\text{VO}(\text{PO}_4)_2$ and $\text{SrZnVO}(\text{PO}_4)_2$ respectively. The good quality of the samples is evident by the absence of any trace of impurity tails at the lowest attainable temperatures, which is typical of paramagnetic foreign phases. Kinks in $\chi(T)$ indicate the onset of magnetic ordering at the Néel temperatures $T_N \sim 3.7 \text{ K}$ and 2.6 K for $\text{Pb}_2\text{VO}(\text{PO}_4)_2$ and $\text{SrZnVO}(\text{PO}_4)_2$ respectively. The fits of the Curie-Weiss law to the high-temperature data ($T > 50 \text{ K}$) are shown as insets in Fig. 3. The effective moments $\mu_{\text{eff}} = (1.72 \pm 0.02)$ are consistent with the predicted value for $S = 1/2$, $\mu_{\text{eff}} = 1.73$. The extrapolated intercepts with the temperature axis give $\theta_{\text{CW}} = J_1 + J_2 = (4.5 \pm 1) \text{ K}$ and $(1.5 \pm 1) \text{ K}$ for $\text{Pb}_2\text{VO}(\text{PO}_4)_2$ and $\text{SrZnVO}(\text{PO}_4)_2$ respectively. The values of θ_{CW} are rather small compared to the positions of the maxima in the susceptibilities T_{Max} , which allow the overall energy scales of the systems J_c to be estimated. This suggests that J_1 and J_2 have opposite signs, providing evidence of mixed FM and AF exchange couplings [6]. The conclusions from the susceptibility measurements for the two compounds are summarized in the phase diagram of Fig. 1. The observed value of θ_{CW} defines a straight

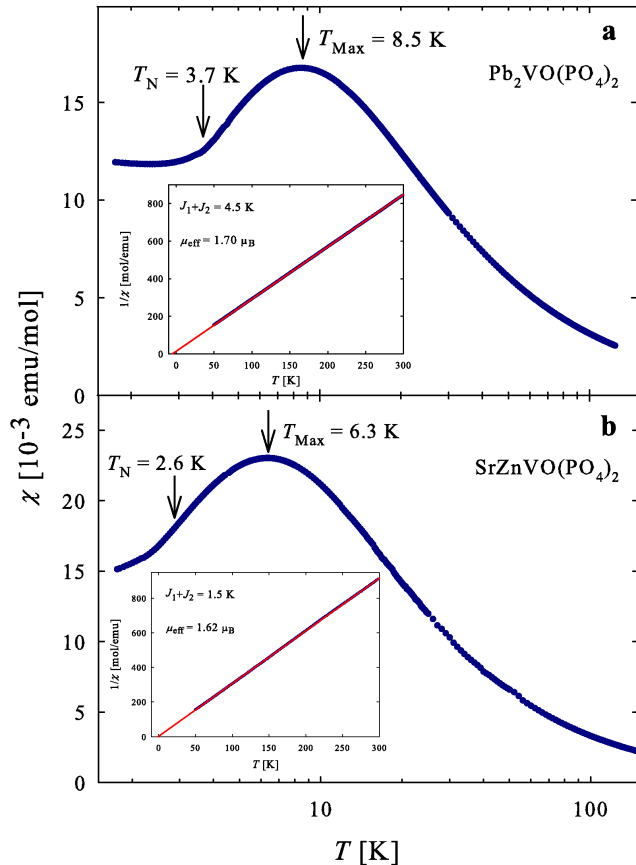


FIG. 3: Magnetic response of polycrystalline (a) $\text{Pb}_2\text{VO}(\text{PO}_4)_2$ and (b) $\text{SrZnVO}(\text{PO}_4)_2$ as measured at 1000 Oe. The broad peaks of $\chi(T)$ are characteristic for low dimensional spin systems. The magnetic phase transitions at T_N manifest as a change of slope in $\chi(T)$, while T_{Max} indicate the energy scale for these systems. Insets show inverse susceptibilities for $T > 50$ K, together with the Curie-Weiss law fits (solid lines), giving $\theta_{\text{CW}} = (4.5 \pm 1)$ K and $\theta_{\text{CW}} = (1.5 \pm 1)$ K for $\text{Pb}_2\text{VO}(\text{PO}_4)_2$ and $\text{SrZnVO}(\text{PO}_4)_2$ respectively.

line on this plot, while the relation between T_{Max} and J_c , which has been calculated in Ref. [6], enables us to get a pair of solutions on this line. Thus for both compounds, there is one possible solution in the CAF and another in the NAF region of the phase diagram.

The neutron scattering experiment complemented these bulk property results, yielding a unique solution in each case. All of the scattering in Fig. 4 is magnetic, and it has been placed on an absolute scale by reference to a standard vanadium sample. At temperatures below the Néel point, the magnetic scattering consists of sharp magnetic Bragg reflections on top of a diffuse magnetic background. Data for powdered samples of $\text{Pb}_2\text{VO}(\text{PO}_4)_2$, $\text{SrZnVO}(\text{PO}_4)_2$, as well as a control sample of $\text{Li}_2\text{VOSiO}_4$ were collected at 1.5 K and were all found to have a CAF structure. This immediately selects

only one of the two solutions consistent with the bulk magnetization data. Fig. 4a shows the magnetic ground state diffraction pattern of $\text{Pb}_2\text{VO}(\text{PO}_4)_2$, modelled by both a CAF structure with an ordering wavevector of $\mathbf{Q} = (\pi, 0)$ (solid line) and a Néel structure for comparison (dashed line that fails to reproduce the data). The ordered moments in the CAF structures are $(0.42 \pm 0.04 \mu_B)$ for $\text{SrZnVO}(\text{PO}_4)_2$, $(0.50 \pm 0.04 \mu_B)$ for $\text{Pb}_2\text{VO}(\text{PO}_4)_2$, and $(0.55 \pm 0.04 \mu_B)$ for $\text{Li}_2\text{VOSiO}_4$. As the ordered moment in the ground state decreases for this series of compounds, the integrated intensity under the diffuse component was found to increase.

Exchange constants are usually determined via the excitations from the ordered phase. However, the large single-crystal samples required for inelastic neutron scattering were not available for any of these compounds. The novelty in our approach was to model $S(Q)$ in polycrystalline materials by using HTSE of the static susceptibility. In the determination of the NN and NNN exchange constants we used the 1st order HTSE given by:

$$S(\mathbf{Q}) \sim S(S+1) \left[1 + \frac{S(S+1)}{3} \cdot \frac{J(\mathbf{Q})}{kT} \right] \cdot F^2(\mathbf{Q}) \quad (2)$$

where S is the spin of the magnetic ions, $F^2(\mathbf{Q})$ the magnetic form factor of the individual magnetic ions and $J(\mathbf{Q})$ is the Fourier transform of the exchange interactions [29]. Fig. 4b shows the diffuse neutron scattering intensity at $T = 20$ K, a temperature well into the paramagnetic phase for this compound. Although magnetic long range order has been destroyed at this temperature, the kT term has not completely washed out all magnetic interactions. The presence of oscillations in the data indicates the existence of short-range spin correlations. Note that we have measured and fixed $F^2(\mathbf{Q})$ directly at room temperature, where no oscillations are present and these systems are ideal paramagnets. The calculated scattering from the two pairs of J 's in Fig. 1 are shown in Fig. 4b. Our results again select the unique solution in the CAF region, with FM $J_1 = (-3.2 \pm 1)$ K and AF $J_2 = (7.7 \pm 1)$ K. Similarly, for $\text{SrZnVO}(\text{PO}_4)_2$, the combined neutron and susceptibility measurements yield $J_1 = (-4.6 \pm 1)$ K (FM) and $J_2 = (6.1 \pm 1)$ K (AF). Note that a similar analysis for $\text{Li}_2\text{VOSiO}_4$ was not possible due to absorption of neutrons by the sample.

The ordered moments in the ground states are smaller than the nominal value for $S = 1/2$ systems due to quantum fluctuations. The value for $\text{Li}_2\text{VOSiO}_4$ is consistent with Ref. [15]. However, the values for $\text{Pb}_2\text{VO}(\text{PO}_4)_2$ and $\text{SrZnVO}(\text{PO}_4)_2$ are significantly lower, indicating an increase in quantum disorder. This is entirely consistent with the fact that values of J_1 and J_2 determined in this study place them successively closer to the disordered region of the phase diagram.

In summary, we have unambiguously determined the exchange constants that are key to understanding a new

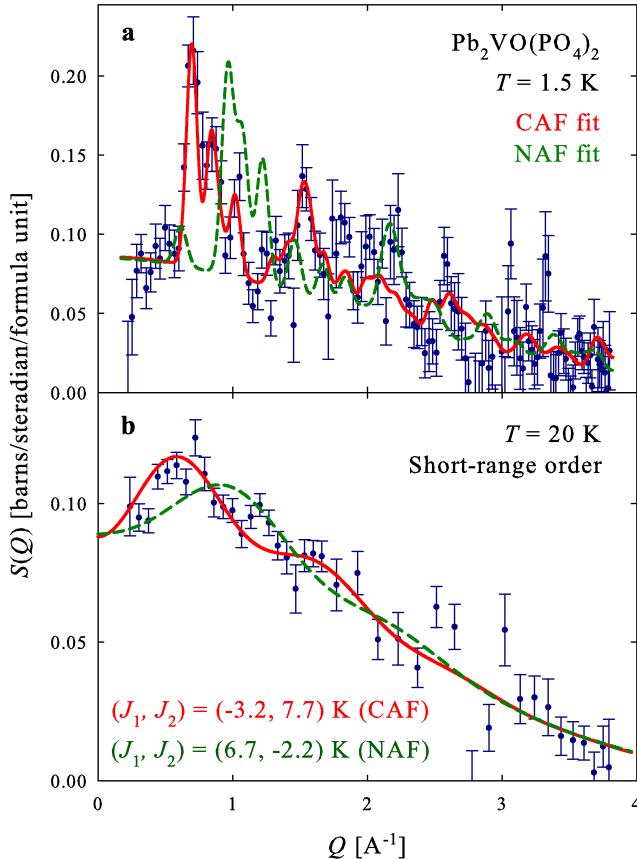


FIG. 4: (a) Magnetic ground state diffraction pattern of $\text{Pb}_2\text{VO}(\text{PO}_4)_2$ measured at 1.5 K. The ordered component of the ions' moments gives rise to sharp magnetic Bragg reflections, while the disordered component gives a diffuse background. Fits are a CAF model with $\mathbf{Q} = (\pi, 0)$ (solid line) as well as a Néel model (dashed line, for comparison only). Part (b) shows short-range spin correlations in the paramagnetic phase of $\text{Pb}_2\text{VO}(\text{PO}_4)_2$. The solid curve is a first-order HTSE calculation for the CAF solution with FM $J_1 = (-3.2 \pm 1)$ K and AF $J_2 = (7.7 \pm 1)$ K, and the dashed is the NAF solution. The data clearly favor the CAF solution.

region of the $J_1 - J_2$ phase diagram with FM NN interactions and AF NNN interactions. We are able to tie down the exchange constants using novel polarized neutron scattering techniques from powdered samples. The reduced ordered moment and increased diffuse magnetic signal indicate the approach to a quantum disordered spin-nematic region. It should be possible to tune the exchange to be closer to the quantum disordered region by other chemical substitutions, or by the application of pressure or magnetic field. These low energy scale systems are particularly well suited for fur-

ther experimental study, for example in high magnetic fields [30, 31], and the polarized neutron scattering techniques described here open new vistas for the exploration of these model magnetic systems.

* Electronic address: markos.skoulatos@helmholtz-berlin.de

- [1] G. Misguich and C. Lhuillier, *Frustrated Spin Systems* (Edited by H.T. Diep, World Scientific, Singapore, 2004).
- [2] Y. Kamihara et al., *J. Am. Chem. Soc.* **130**, 3296 (2008).
- [3] X. H. Chen et al., *Nature* **453**, 761 (2008).
- [4] Q. Si and E. Abrahams, *Phys. Rev. Lett.* **101**, 076401 (2008).
- [5] H. J. Schulz, T. A. L. Ziman, and D. Poilblanc, *J. Phys. I France* **6**, 675 (1996).
- [6] N. Shannon et al., *Eur. Phys. J. B* **41**, 599 (2004).
- [7] N. Shannon, T. Momoi, and P. Sindzingre, *Phys. Rev. Lett.* **96**, 027213 (2006).
- [8] P. Millet and C. Satto, *Materials Research Bulletin* **33**, 1339 (1998).
- [9] R. Melzi et al., *Phys. Rev. Lett.* **85**, 1318 (2000).
- [10] R. Melzi et al., *Phys. Rev. B* **64**, 024409 (2001).
- [11] P. Carretta, R. Melzi, N. Papinutto, and P. Millet, *Phys. Rev. Lett.* **88**, 047601 (2002).
- [12] P. Carretta et al., *Phys. Rev. B* **66**, 094420 (2002).
- [13] H. Rosner et al., *Phys. Rev. Lett.* **88**, 186405 (2002).
- [14] H. Rosner, R. R. P. Singh, W. H. Zheng, J. Oitmaa, and W. E. Pickett, *Phys. Rev. B* **67**, 014416 (2003).
- [15] A. Bombardi et al., *Phys. Rev. Lett.* **93**, 027202 (2004).
- [16] A. Bombardi et al., *Phys. Rev. B* **71**, 220406(R) (2005).
- [17] A. A. Tsirlin et al., *Phys. Rev. B* **77**, 092402 (2008).
- [18] K. Oka et al., *Inorg. Chem.* **47**, 7355 (2008).
- [19] E. E. Kaul et al., *J. Magn. Magn. Mater.* **272-276**, 922 (2004).
- [20] R. V. Shpanchenko et al., *Acta Cryst. C*, **62**, i88 (2006).
- [21] M. Skoulatos et al., *J. Magn. Magn. Mater.* **310**, 1257 (2007).
- [22] R. Nath, A. A. Tsirlin, H. Rosner, and C. Geibel, *Phys. Rev. B* **78**, 064422 (2008).
- [23] H. Kageyama et al., *J. Phys. Soc. Jpn.* **74**, 1702 (2005).
- [24] N. Oba et al., *J. Phys. Soc. Jpn.* **75**, 113601 (2006).
- [25] P. Thalmeier, M. E. Zhitomirsky, B. Schmidt, and N. Shannon, *Phys. Rev. B* **77**, 104441 (2008).
- [26] O. Schärpf and H. Capellmann, *Phys. Stat. Sol.* **A135**, 359 (1993).
- [27] E. E. Kaul, "Experimental Investigation of New Low-Dimensional Spin Systems in Vanadium Oxides" (PhD Thesis, Technische Universität Dresden, Dresden, 2005).
- [28] S. Meyer and B. Mertens and Hk. Müller-Buschbaum, *Zeitschrift für Naturforschung* **52b**, 985 (1997).
- [29] N. W. Ashcroft and N. D. Mermin, *Solid State Physics*, ch. 33 (Holt-Saunders International Editions, 1976).
- [30] B. Schmidt, N. Shannon, and P. Thalmeier, *J. Phys.: Condens. Matter* **19**, 145211 (2007).
- [31] B. Schmidt, P. Thalmeier, and N. Shannon, *Phys. Rev. B* **76**, 125113 (2007).